Electronic Supplementary Material (ESI) for Nanoscale.

Supporting Information: Molecular Dynamics Study on Ion-mediated Self-assembly of Monolayer-protected Nanoclusters

Vikas Tiwari, Anushna Bhattacharyya, and Tarak Karmakar*

Department of Chemistry, Indian Institute of Technology, Delhi, Hauz Khas, New Delhi 110016, India

E-mail: tkarmakar@chemistry.iitd.ac.in

Contents

S1 System setup

The structure and topology of the MPCs were obtained from the nanomodeler server.[S1] A cubic box of edge length ~ 8 nm was used to simulate the monomer and dimer of $Au_{25}(p\text{MBA})_{18}$ and $Au_{25}(\text{DPA})_{18}$ MPCs in TIP3P water. GROMACS[S2] in-built tools were used to prepare the systems with the Zn^{2+} and monovalent Ch^{+} and TEA^{+} ions. Cl^{-} ions were used to neutralize the system.

S2 Simulation details

All simulations were conducted using GROMACS[S2] version 2021.4, which was patched with PLUMED[S3–S5] version 2.8.0 to enable enhanced sampling techniques. The systems were initially minimized using the steepest descent algorithm to relieve any steric clashes or high-energy configurations. Subsequently, the systems were thermally equilibrated at 300 K in the canonical (NVT) ensemble. Pressure equilibration to 1 bar was achieved using the isothermal-isobaric (NPT) ensemble after 1 ns of simulation. Temperature control was achieved using the stochastic velocity rescaling thermostat[S6] with a temperature coupling constant of 0.5 ps. The pressure was maintained constant at 1 bar using the isotropic Parrinello-Rahman barostat.[S7] Van der Waals and short-range Coulombic interactions were truncated at a cut-off distance of 1.0 nm. Long-range electrostatic interactions were treated using the Particle Mesh Ewald (PME) approach. Production simulations were conducted in the NPT ensemble with a time step of 2 fs. Covalent bonds containing hydrogen atoms were constrained during production runs using the LINCS algorithm.[S8] Simulation trajectories were visualized using VMD software,[S9] and figures and movies were produced accordingly. Analysis of simulation data was performed using built-in GROMACS tools, the PLUMED driver, and in-house Python scripts. Furthermore, metadynamics and on-the-fly probability-based enhanced sampling (OPES) simulations were conducted using the PLUMED plugin within the GROMACS software, allowing for the exploration of complex energy landscapes and rare events.

S3 Effect of $R_{Zn^{2+}/ligands}$ ratio on dimerization of Au-DPA MPC

To investigate the impact of the ratio of Zn^{2+} ions to ligands ($R_{Zn^{2+}/ligands}$) on dimerization, simulations were conducted with $R_{Zn^{2+}/ligands}$ values of 0.0, 0.3, 0.5, 1.0, and 2.0. In the absence of Zn^{2+} ($R_{Zn^{2+}/ligands} = 0.0$), electrostatic repulsion between ligands prevented the Au-DPA monomers from approaching each other to form a dimer. Even with $R_{Zn^{2+}/ligands}$ set to 0.3, dimerization did not occur within 100 ns of simulation, as illustrated in Fig. S1. Sodium ions (Na^+) were used to neutralize the systems when $R_{Zn^{2+}/ligands}$ was set to 0.0 and 0.3. Notably, Na^+ exhibited an inhibitory effect on aggregation, consistent with previous experimental findings.[S10] Dimer formation was observed with $R_{Zn^{2+}/ligands} = 0.5$ after approximately 50 ns, maintaining stability throughout the 100 ns simulation. At this concentration, a charge balance existed between Zn^{2+} and ligands. Moreover, dimerization occurred more rapidly with $R_{Zn^{2+}/ligands}$ values of 1.0 and 2.0, taking approximately 3 ns and 12 ns, respectively, as depicted in Fig. S1. These results indicate that dimerization only occurs beyond a threshold $R_{Zn^{2+}/ligands}$ value.

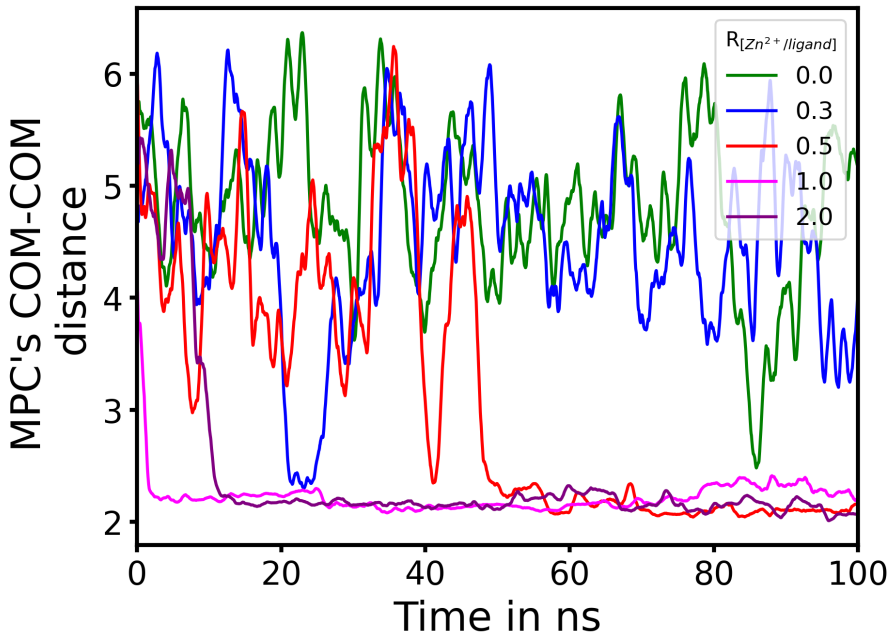

Figure S1: MPC's COM-COM distance vs. simulation time at different $R_{Zn^{2+}/ligands}$.

S4 Well-tempered MetaD simulation - dimerization of Au-DPA

To investigate the stability of the formed dimer and the thermodynamics underlying Zn^{2+}'s influence on dimer formation, we conducted WT-MetaD simulations utilizing two collective variables (CVs) adept at distinguishing between monomeric and dimeric states. As the system transitions from monomeric to dimeric, the COM distance between the Au-DPA MPCs (s_1) decreases while s_2, representing the interfacial Zn^{2+} coordination number, increases. Fig. S2 depicts s_1 plotted against simulation time, with the color bar denoting the metadynamics bias, effectively capturing the multiple transitions between monomeric and dimeric states.

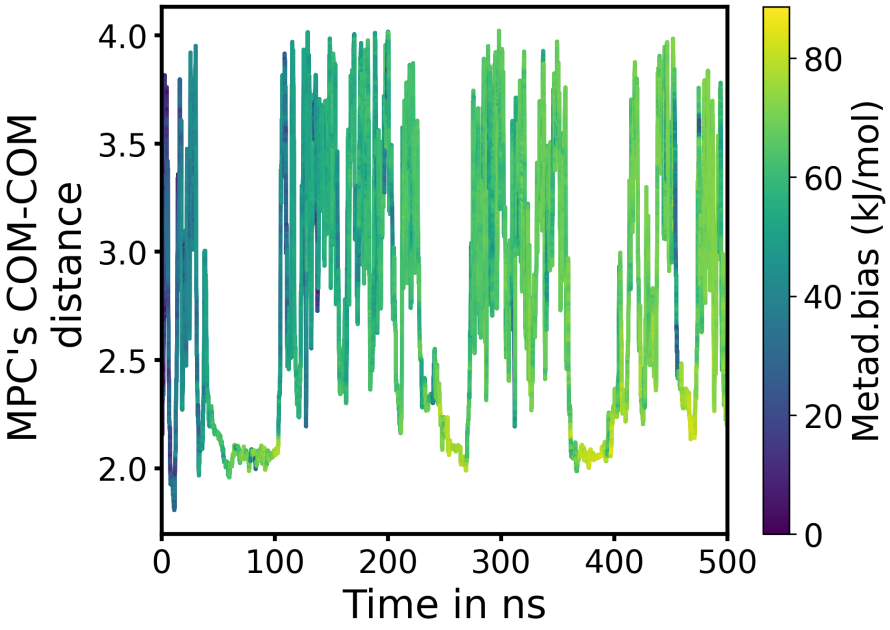

Figure S2: s_1 vs simulation time with color bar denoting the metadynamics bias.

S5 Dimerization of Au-MPCs in the presence of Cd^{2+} ions

In the cation-mediated self-assembly of Au-MPCs in the presence of Cd^{2+}, results were similar to those observed with Zn^{2+}, with one notable difference found in the radial distribution function (RDF) plot. Specifically, a strong correlation was observed between Cd^{2+} and the 'O' of COO^- at approximately 0.2 nm distance, indicating the presence of Cd^{2+} ions in the first coordination shell of 'O' (as depicted in Fig. S3a), a feature not observed with Zn^{2+} (Fig. S3d). Further elaboration on this discrepancy is provided in the subsequent section.

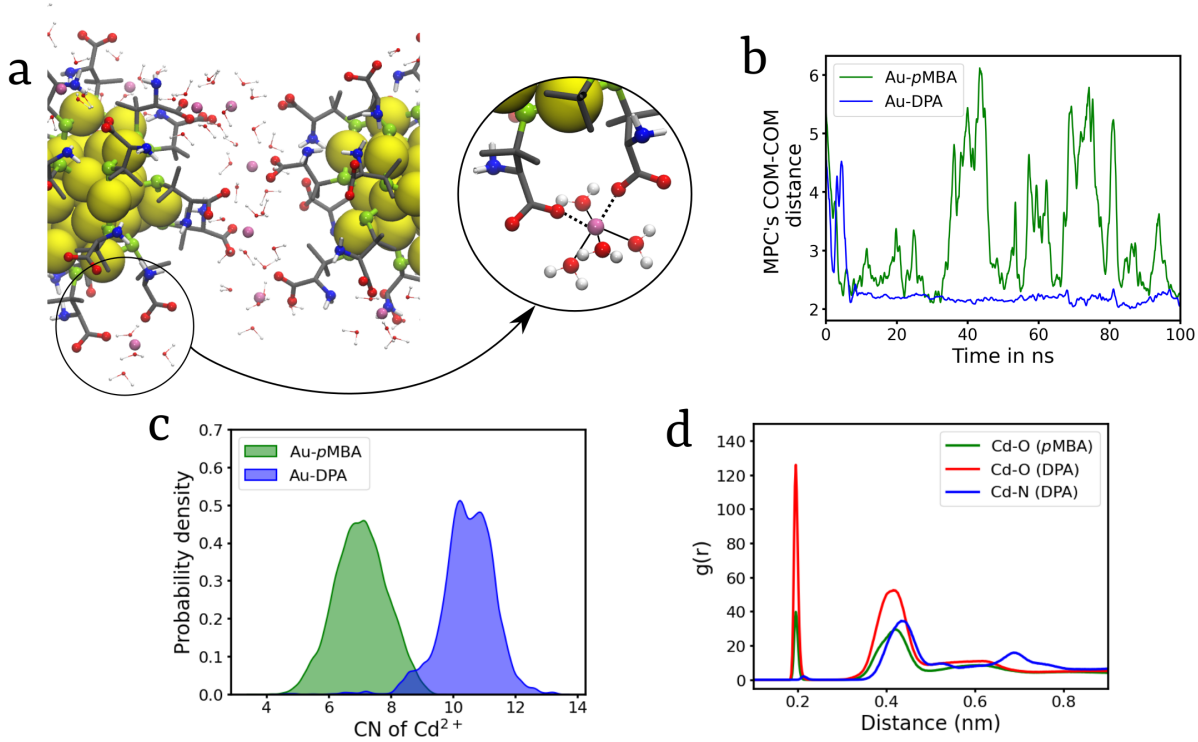

Figure S3: (a) Snapshot of the interaction of Cd^{2+} with Au-DPA (Inset: Cd^{2+} interacting with carboxylate ligands in its 1^{st} coordination shell), (b) MPC's COM-COM distance vs time, (c) coordination number distribution analysis, (e) radial distribution function analysis.

Further to understand the energetics of Au-DPA MPCs dimerization, we carried out a Well-tempered metadynamics (WTMetaD) simulation using two collective variables, s_1 is the COM-COM distance between the MPCs, and s_2 is the interfacial Cd^{2+} coordination number. The reweighted free energy surface is plotted on the two collective variables (s_1 and s_2) space (Fig. S4). The Au-DPA dimer is stable by ~20 kJ/mol with a negligible barrier

for the monomer to dimer transition.

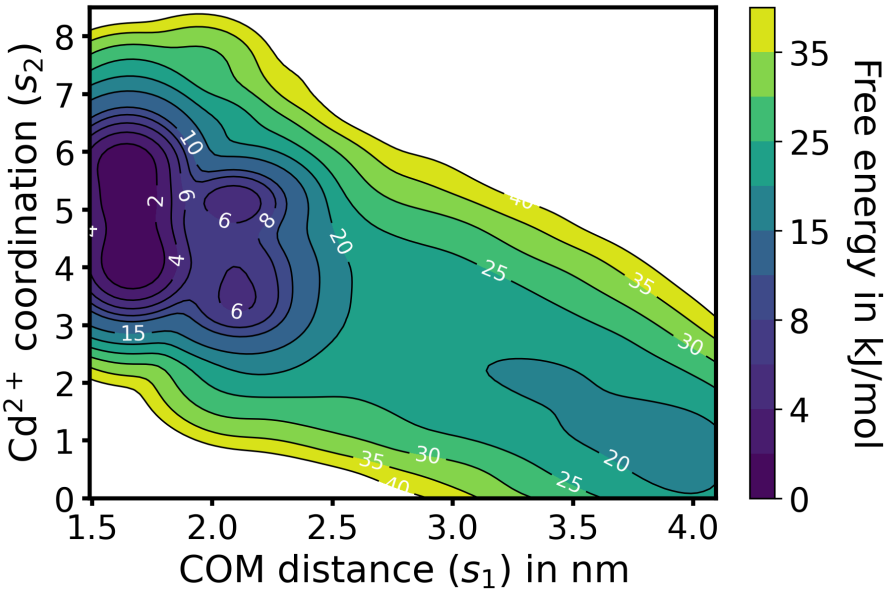

Figure S4: Free energy profile for dimerization of $Au_{25}(DPA)_{18}$ in the presence of Cd^{2+} ions.

S6 OPES$_E$ simulations of acetate-M^{2+} (M = Zn, Cd) system

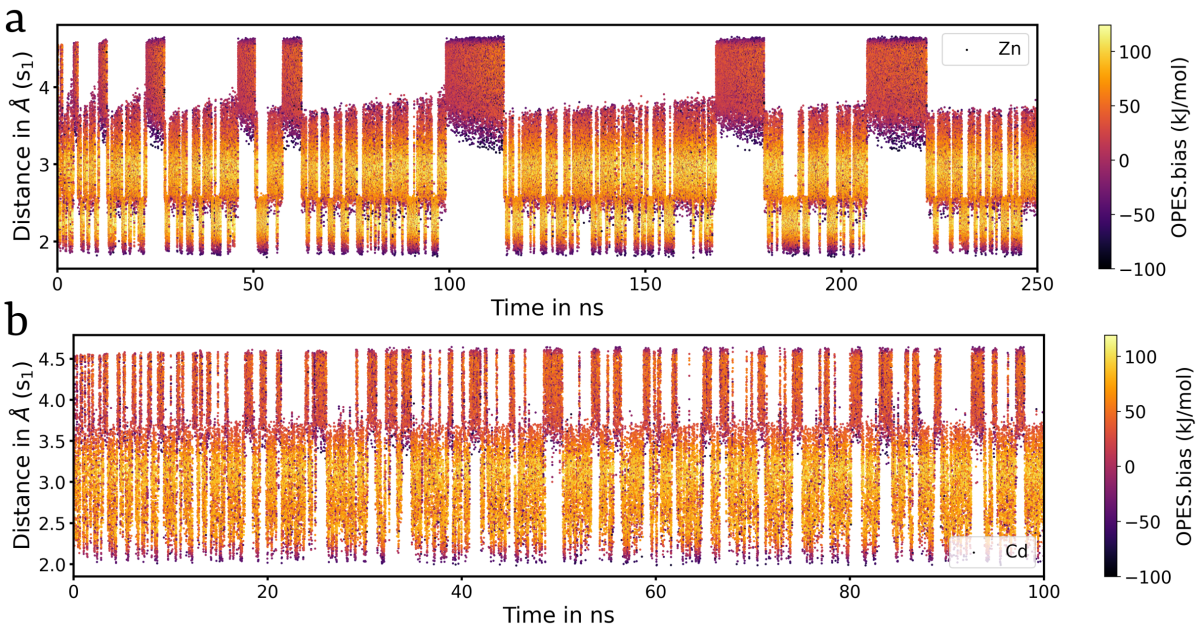

Figure S5: s_1 vs simulation time with color bar denoting the opes.bias for: (a) acetate-Zn^{2+} and (b) acetate-Cd^{2+}.

To investigate the energetics of M^{2+}-COO^- (M = Zn, Cd) coordination, we conducted a small-scale experiment using a system comprising an acetate molecule and a M^{2+} ion, neutralized with a Cl^- ion. Following equilibration, on-the-fly probability enhanced sampling (OPES$_E$, explore variant)[S11,S12] simulations were performed employing two collective variables: s_1, representing the distance between the Zn and carboxylate carbon (COO) of the acetate molecule, and s_2, indicating the number of water molecules in the first coordination sphere of the M^{2+}. The OPES$_E$ simulations were performed using adaptive Gaussian width (σ) and the energy was regulated using a barrier height of 100 kJ/mol. The simulations revealed multiple back-and-forth transitions between various metastable states (Fig. S5). Subsequently, the unbiased underlying free energy profile was obtained through bias reweighting methods. Three metastable states — singly-bound (Zn-O), doubly-bound (O-Zn-O), and unbound were identified (Fig. S6). A Gibbs free energy barrier of $\sim$ 25 kJ/mol (for Zn^{2+}) was observed to transition from the unbound state to the bound state, with

a slightly lower barrier of 22 kJ/mol observed for Cd^{2+}. This suggests that in the case of Cd^{2+}, a few ions can overcome the smaller energy barrier and move into the first coordination sphere of the carboxylate oxygen (as observed from Fig. S3d).

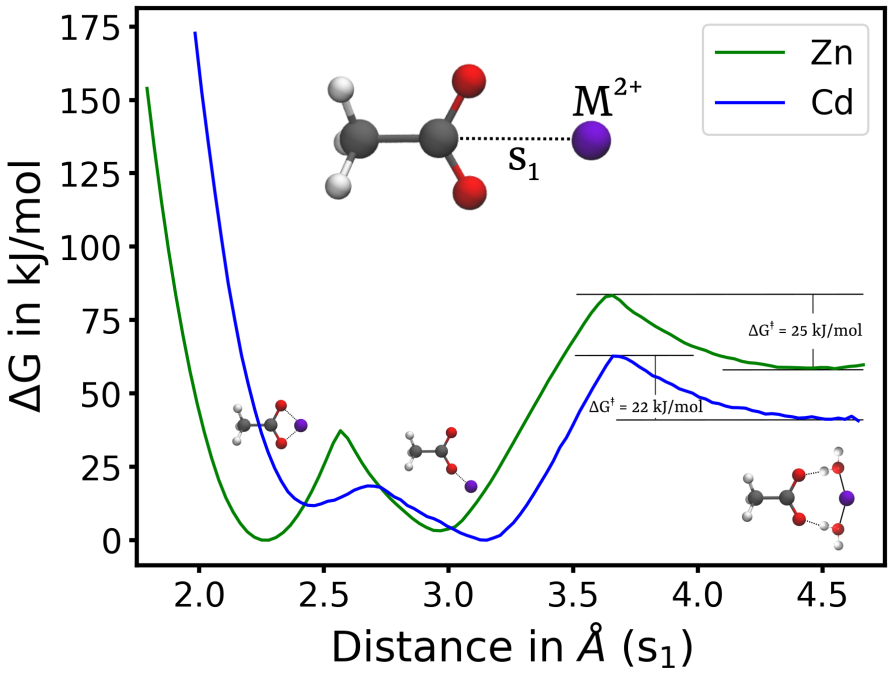

Figure S6: Free energy (ΔG) profile showing various coordination states of Zn^{2+} (green) and Cd^{2+} (blue) as a function of CV s_1 (distance between the cation (Zn^{2+}, Cd^{2+}) and the caboxylate carbon of acetate).

S7 Effect of $R_{M^{2+}/ligands}$ on self-assembly

Simulations of 20 randomly dispersed Au-DPA MPCs at $R_{Zn^{2+}/ligands}$ = 0.3, 0.5 and 1.0. To compare the effect of Cd^{2+} ions, a simulation with Cd^{2+} ions were carried out at $R_{Cd^{2+}/ligands}$ = 0.5. As expected similar self-assembly pattern were observed (Fig. S8d). Fig. S8 depicts the evolution of the MPCs cluster with the simulation time. DFS cluster analysis showed formation of largest cluster of 10 MPCs within 300 ns of the simulation in contrast to the case of zinc. This maybe be due to the larger size of the cadmium, which hinders the clustering of small cluster into bigger one.

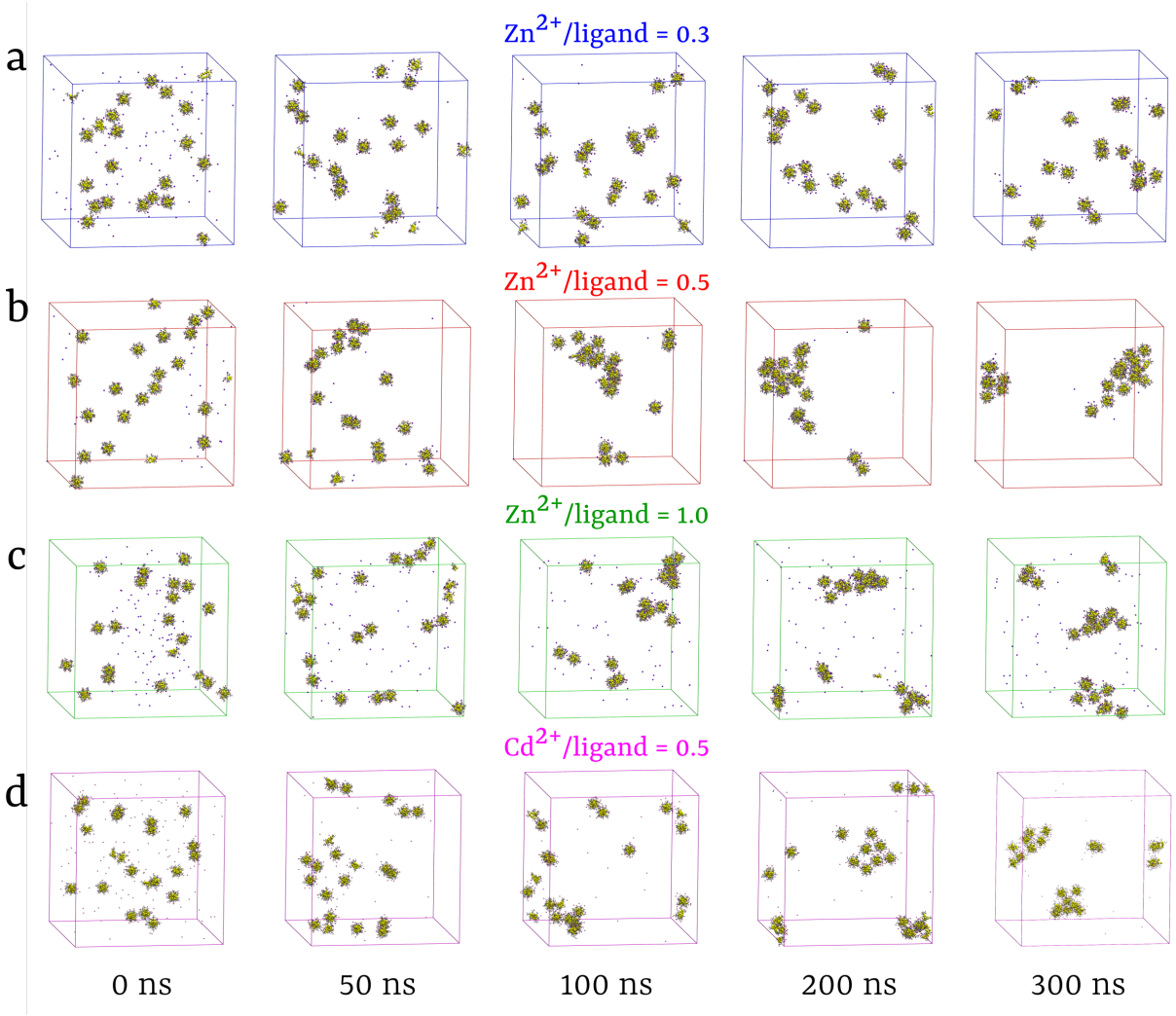

Figure S7: Snapshots of the 20 randomly dispersed MPCs taken at different time intervals showing the self-assembly process at $R_{Zn^{2+}/ligands}$ = (a) 0.3, (b) 0.5, (c) 1.0 and (d) $R_{Cd^{2+}/ligands}$ = 0.5

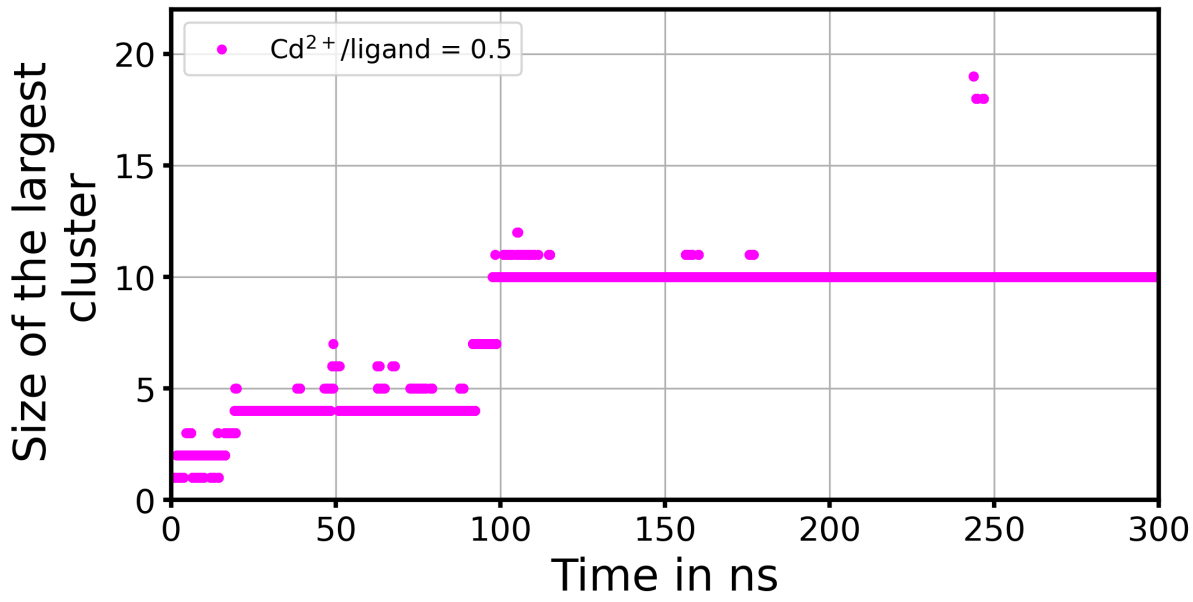

Figure S8: DFS cluster analysis showing the size of largest cluster with respect to simulation time.

S8 Effect of TEA^+ ions on dimerization of Au-MPCs

Similar to Ch^+ cations, TEA^+ also adsorbs onto the Au-*p*MBA surface (Fig. S9a). However, due to the bulky nature of the DPA ligand, TEA^+ interacts weakly with Au-DPA MPCs (Fig. S9b). Analysis of the MPCs' center-of-mass distance plot (Fig. S9c) reveals the inhibitory effect of TEA^+. Specifically, Au-*p*MBA exhibits a high coordination number of TEA^+ ions, while Au-DPA shows a significantly lower number of coordinated TEA^+ ions (Fig. S9d). Additionally, radial distribution function (RDF) analysis (Fig. S9e) demonstrates a strong correlation between the nitrogen of TEA^+ and the oxygen of *p*MBA, whereas a negligible correlation is observed with the oxygen of DPA.

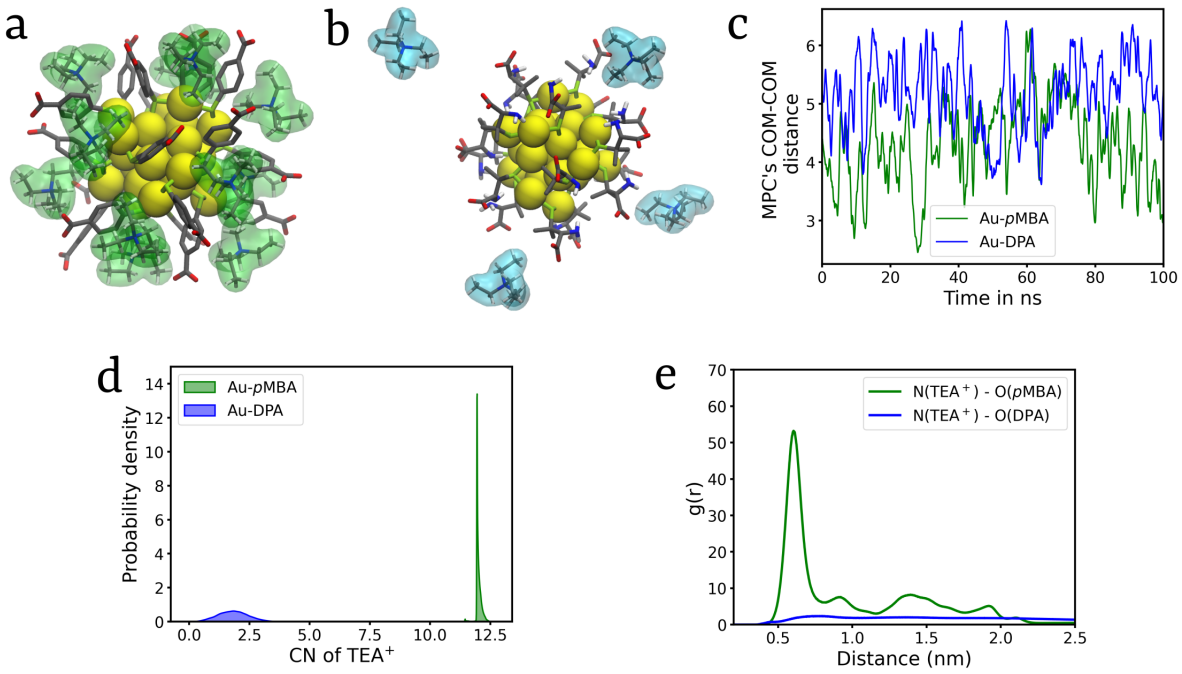

Figure S9: (a) TEA^+ ions interactions with Au-*p*MBA, (b) TEA^+ ions interactions with Au-DPA, (c) MPC's COM-COM distance vs time, (d) coordination number distribution analysis, (e) radial distribution function analysis.

S8.1 Simulation of multimeric system in the presence of Ch^+ and TEA^+

Conforming to our research outcomes from the dimerization of Au-MPCs in the presence of Ch^+ and TEA^+, we simulate a multimeric system consisting of 20 randomly dispersed Au-

DPA MPCs in water. In line with the aforementioned results, we observe the predominating nature of inhibition. On employing the DFS clustering algorithm to monitor the evolution of clusters, the analysis reflects the same constrictive effect in the presence of both the molecular cations (Fig. S10).

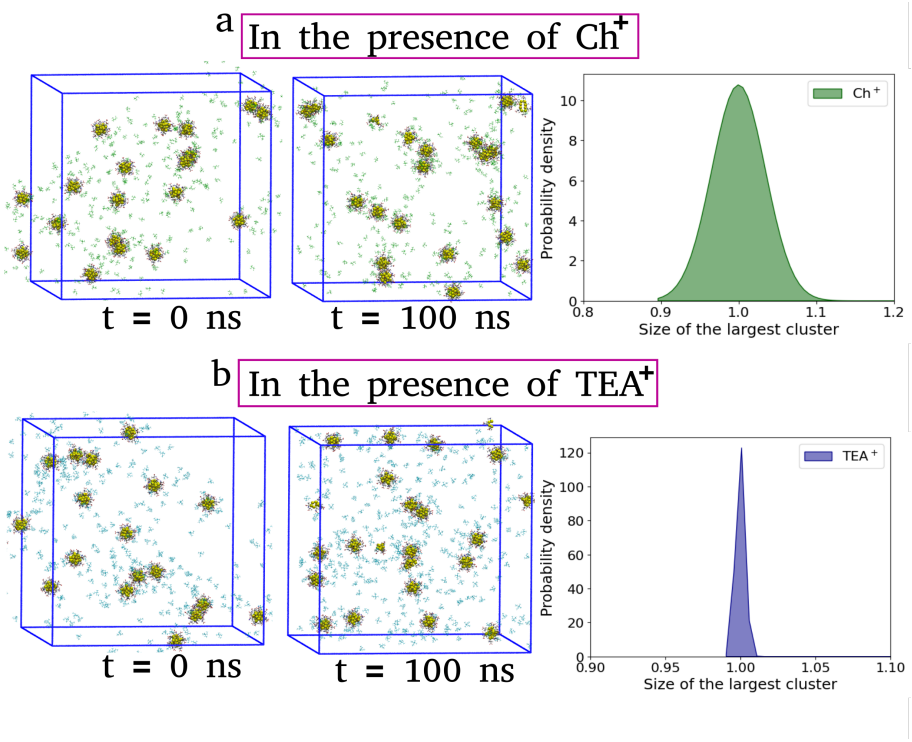

Figure S10: (a) Snapshots of the initial and final frame depicting the inhibitory effect of Ch^+, DFS cluster analysis showing the size of largest cluster (b) Snapshots of the initial and final frame depicting the inhibitory effect of TEA^+, DFS cluster analysis showing the size of largest cluster.

References

(S1) Franco-Ulloa, S.; Riccardi, L.; Rimembrana, F.; Pini, M.; De Vivo, M. NanoModeler: A Webserver for Molecular Simulations and Engineering of Nanoparticles. *Journal of Chemical Theory and Computation* **2019**, *15*, 2022–2032.

(S2) Berendsen, H.; van der Spoel, D.; van Drunen, R. GROMACS: A message-passing parallel molecular dynamics implementation. *Computer Physics Communications* **1995**, *91*, 43–56.

(S3) Promoting transparency and reproducibility in enhanced molecular simulations. *Nature Methods* **2019**, *16*, 670–673.

(S4) Tribello, G. A.; Bonomi, M.; Branduardi, D.; Camilloni, C.; Bussi, G. PLUMED 2: New feathers for an old bird. *Computer Physics Communications* **2014**, *185*, 604–613.

(S5) Bonomi, M.; Branduardi, D.; Bussi, G.; Camilloni, C.; Provasi, D.; Raiteri, P.; Donadio, D.; Marinelli, F.; Pietrucci, F.; Broglia, R. A.; Parrinello, M. PLUMED: A portable plugin for free-energy calculations with molecular dynamics. *Computer Physics Communications* **2009**, *180*, 1961–1972.

(S6) Bussi, G.; Donadio, D.; Parrinello, M. Canonical sampling through velocity rescaling. *Chem. Phys.* **2007**, *126*.

(S7) Parrinello, M.; Rahman, A. Polymorphic transitions in single crystals: A new molecular dynamics method. *Journal of Applied Physics* **1981**, *52*, 7182–7190.

(S8) Hess, B.; Bekker, H.; Berendsen, H. J. C.; Fraaije, J. G. E. M. LINCS: A linear constraint solver for molecular simulations. *Journal of Computational Chemistry* **1997**, *18*, 1463–1472.

(S9) Humphrey, W.; Dalke, A.; Schulten, K. VMD: Visual molecular dynamics. *Journal of Molecular Graphics* **1996**, *14*, 33–38.

(S10) Yao, Q.; Luo, Z.; Yuan, X.; Yu, Y.; Zhang, C.; Xie, J.; Lee, J. Y. Assembly of nanoions via electrostatic interactions: ion-like behavior of charged noble metal nanoclusters. *Scientific Reports* **2014**, *4*, 3848.

(S11) Invernizzi, M.; Parrinello, M. Rethinking Metadynamics: From Bias Potentials to Probability Distributions. *The Journal of Physical Chemistry Letters* **2020**, *11*, 2731–2736.

(S12) Invernizzi, M.; Parrinello, M. Exploration vs Convergence Speed in Adaptive-Bias Enhanced Sampling. *Journal of Chemical Theory and Computation* **2022**, *18*, 3988–3996.